Molecular Neurobiology (2019) 56:8220–8236
https://doi.org/10.1007/s12035-019-01665-y

Autophagy Induction by Bexarotene Promotes Mitophagy in Presenilin 1 Familial Alzheimer's Disease iPSC-Derived Neural Stem Cells

Patricia Martín-Maestro[1] · Andrew Sproul[2] · Hector Martinez[3] · Dominik Paquet[4] · Meri Gerges[1] · Scott Noggle[3] · Anatoly A. Starkov[1]

Received: 13 March 2019 / Accepted: 30 May 2019 / Published online: 16 June 2019

Abstract

Adult neurogenesis defects have been demonstrated in the brains of Alzheimer's disease (AD) patients. The neurogenesis impairment is an early critical event in the course of familiar AD (FAD) associated with neuronal loss. It was suggested that neurologic dysfunction in AD may be caused by impaired functioning of hippocampal neural stem cells (NSCs). Multiple metabolic and structural abnormalities in neural mitochondria have long been suspected to play a critical role in AD pathophysiology. We hypothesize that the cause of such abnormalities could be defective elimination of damaged mitochondria. In the present study, we evaluated mitophagy efficacy in a cellular AD model, hiPSC-derived NSCs harboring the FAD-associated *PS1* M146L mutation. We found several mitochondrial respiratory chain defects such as lower expression levels of cytochrome c oxidase (complex IV), cytochrome c reductase (complex III), succinate dehydrogenase (complex II), NADH:CoQ reductase (complex I), and also ATP synthase (complex V), most of which had been previously associated with AD. The mitochondrial network morphology and abundance in these cells was aberrant. This was associated with a marked mitophagy failure stemming from autophagy induction blockage, and deregulation of the expression of proteins involved in mitochondrial dynamics. We show that treating these cells with autophagy-stimulating drug bexarotene restored autophagy and compensated mitochondrial anomalies in PS1 M146L NSCs, by enhancing the clearance of mitochondria. Our data support the hypothesis that pharmacologically induced mitophagy enhancement is a relevant and novel therapeutic strategy for the treatment of AD.

Keywords Alzheimer's disease · Presenilin 1 · Mitophagy · hiPSC-derived neural stem cells · Bexarotene

Electronic supplementary material The online version of this article (https://doi.org/10.1007/s12035-019-01665-y) contains supplementary material, which is available to authorized users.

✉ Patricia Martín-Maestro
pam2066@med.cornell.edu

Andrew Sproul
aas2003@cumc.columbia.edu

Hector Martinez
HMartinez@NYSCF.org

Dominik Paquet
dominik.paquet@med.uni-muenchen.de

Meri Gerges
meg2016@med.cornell.edu

Scott Noggle
snoggle@NYSCF.org

Anatoly A. Starkov
ans2024@med.cornell.edu

[1] Feil Family Brain and Mind Research Institute, Weill Cornell Medicine, New York, NY, USA

[2] Department of Pathology & Cell Biology and the Taub Institute for Research on Alzheimer's Disease and the Aging Brain, Columbia University, New York, NY, USA

[3] The New York Stem Cell Foundation, New York, NY, USA

[4] Institute for Stroke and Dementia Research (ISD), University Hospital, LMU Munich, Germany

Background

Alzheimer's disease (AD) is the most prevalent neurodegenerative disease and the leading cause of dementia characterized by several histopathological markers including extracellular amyloid plaques, neurofibrillary tangles within neurons, the loss of synaptic connections manifested as brain atrophy, and neuroinflammation [1, 2]. Early-onset, dominantly inherited forms of AD (familiar AD, abbreviated as "FAD") are associated with more than 200 mutations in the amyloid precursor protein [3] or the presenilin 1 and 2 genes (*PS1/2*) [4]. Of those, mutations in the *PS1* gene, located on chromosome 14, occur most frequently in FAD. Defective PS1 interferes with the function of the γ-secretase complex, which alters the processing of the APP and leads to the overproduction of a longer, toxic version of Aβ peptide (Aβ42) that is more oligomerogenic [5]. Generation of toxic Aβ oligomers likely leads to synaptic dysfunction and ultimately the death of neurons.

Adult neurogenesis defects have been described in the brain of patients and in animal models of AD [6, 7], and the neurogenesis impairment is an early critical event in the course of FAD than the onset of hallmark lesions or neuronal loss, at least in mouse models of FAD [8]. It is hypothesized that neurologic dysfunction associated with AD may be caused by impaired functioning of hippocampal neural stem cells (NSCs) [9]. Reduction or dysfunction of PS1 may play a role in neurogenesis [10–12]. It was shown that the deposition of Aβ itself may disrupt this process [13, 14] suggesting, at least partially, a γ-secretase-dependent role of PS1 in neurogenesis [15]. Therefore, strategies to improve NSC survival and function may be beneficial for the treatment of AD.

Mitochondria play multiple important roles in maintaining cell survival, cell death, and cellular metabolic homeostasis. Several studies have demonstrated the crucial role of mitochondrial function in NSC survival and differentiation [16–19]. It was reported that mitochondrial damage increases the levels of mitochondrial ROS production, which then suppresses neurogenesis through mechanisms which include Sirt1 oxidation as well as cell death of NSCs via necrotic or apoptotic signaling activation [20]. Furthermore, mitochondrial dynamics can act as a regulatory factor in the developmental program of NSCs [21]. Mitochondrial dysfunction is believed to play a major role in the development of AD [22]. However, little is known about the role of mitochondrial quality control pathways, such as mitophagy in connecting NSC mitochondrial abnormalities and neurogenesis. Mitophagy is the selective degradation of mitochondria by autophagy. It promotes turnover of mitochondria and prevents accumulation of dysfunctional mitochondria which can lead to cellular degeneration [23]. Parkin-dependent mitophagy is one of the best studied mechanisms for mitophagy in mammalian cells [24]. After mitochondrial damage, PTEN-induced putative kinase 1 (PINK1) is stabilized in the mitochondrial membrane. In turn, Parkin is recruited to the mitochondria [25, 26], where Parkin mediates the ubiquitination of mitochondrial proteins VDAC1 [27] and mitofusins [28]. This results in the recruitment of autophagy adapter proteins, such as sequestosome 1 (SQSTM1/p62), optineurin (OPTN), or NDP52, that mediate the cargo engulfment into autophagosomes by the interaction with MAP1LC3/LC3 (microtubule-associated protein 1 light chain 3) to finally fuse with the lysosomes to degrade their content [29]. The AD-related mitophagy impairment was previously suggested by the accumulation of mitochondria in AD patients [30–33].

Retinoids regulate the expression of numerous genes involved in different cell processes mediated by two classes of receptors, i.e., retinoic acid receptors (RARs) and retinoid X receptors (RXRs). Defective retinoid signaling is well demonstrated in the pathology of AD [34]. Retinoids appear to be promising therapeutic targets for AD treatment through the potential benefits in amyloid modulation, inflammation's suppression, neurotransmission, and neurogenesis. Bexarotene, a synthetic product structurally similar to retinoic acid compounds, is a retinoid X receptor (RXR) agonist approved by the FDA for all stages of cutaneous lymphoma [35]. In addition to targeting the cancer-related genes involved in different cellular mechanisms, this antineoplastic agent stimulated protein biosynthesis and improved the expression of genes related to mitochondrial bioenergetics [36]. Bexarotene has been shown to be beneficial in several models of neurodegenerative diseases including Parkinson's disease, Huntington's disease, amyotrophic lateral sclerosis, and epilepsy [37–39]. In case of AD, several laboratories demonstrated the clearance of soluble Aβ by apolipoprotein E accompanied by reversing memory deficits in a mouse model [40, 41] and AD patients [42, 43]. Furthermore, bexarotene also counteracted the effect of apoE4 on the levels of hyperphosphorylated tau in AD mouse model [44].

In the present work, we evaluated mitophagy failure in iPSC-derived NSCs harboring the FAD-associated *PS1* M146L mutation that had been knocked into both alleles of a control iPSC line, as compared with its isogenic control. PS1 M146L NSCs demonstrated mitochondrial accumulation due to a mitochondrial recycling failure stemming from autophagy induction blockage as well as an aberrant mitochondrial network morphology and a deregulation of the proteins involved in mitochondrial dynamics. We found that bexarotene treatment enhanced autophagy induction and restored mitochondrial network morphology in PS1 M146L NSCs, thereby increasing the removal of accumulated mitochondria. Overall, our data suggest that pharmacological mitophagy enhancement may be a promising therapeutic strategy for treating AD.

Methods

Generation of PS1 M146L Knockin iPSCs and NSC Differentiation

Isogenic iPSC lines used in this study were generated and validated by Andrew Sproul and Scott Noggle from New York Stem Cell Foundation. The 7889(S)B parent control iPSC line was reprogrammed from a control PS1 M146L family fibroblast (PS1 WT/WT; Coriell) using Sendai viral expression of the four canonical Yamanaka factors—Oct4, KLF4, SOX2, and c-Myc (CytoTune, Life), as had been done previously for the same fibroblast line with retroviral reprogramming [45] and has been described in a recent publication [46]. iPSC colonies were initially selected by morphology, passaged several times to remove transformed cells, and expanded before characterization.

The *PS1* M146L was knocked into of 7889(S)B using TALENs targeting exon 5 of *PS1*. TALENs were designed by Dr. Dominik Paquet (Rockefeller University) and generated via FLASH assembly (Rockefeller University Core Facility and Siobhan Gregg). Multiple TALEN pairs were tested for efficacy in 293 cells by transfecting left and right TALENs in different combinations, subsequently amplifying the gDNA region surrounding *PS1* exon 5, and testing for loss of the BspH1 restriction site by NHEJ repair. One of the best TALEN pairs (L3R1) was electroporated into 7889(S)B (15 μg/TALEN; BioRad Xcell) along with 30 μg of a ssDNA template (67 bps; Integrated DNA Technologies) that incorporated the *PS1* M146L mutation and was plated at clonal density. After splitting, one well for each clone was used to isolate gDNA (Qiagen), amplified for *PS1* exon 5, and Sanger sequenced for introduction of the mutation. Homozygous knockin clone G14 was used for further studies along with its isogenic control G4, which remained WT after undergoing targeting.

Undifferentiated iPSCs were cultured on Cultrex (Trevigen, 3432-005-01)-coated dishes and grown in feeder-free maintenance basal medium for hESCs and hiPSCs mTesR1 (StemCell Technologies, 05851) supplemented with mTeSR1 5× Supplement (StemCell Technologies, 05852) and penicillin-streptomycin (100 U/mL–0.1 mg/mL) in a 5% CO_2 in a humid incubator at 37 °C. For neural stem cell differentiation, iPSC colonies were dissociated into single cells by washing with PBS and adding 1 mL Accutase (Life Technologies, A1110501) and then plated onto Matrigel-coated dishes in mTesR1 medium containing 10 μM ROCK inhibitor (Y-27632, Stemgent, 04-0012). Cells were plated at a density of 3×10^5 cells/well in a six-well plate and allowed to recover for 24 h. Then, medium was change to PSC Neural Induction medium (Gibco, A1647801) for neural induction for 7 days, and the media was change every other day. We confirmed the expression of canonical pluripotency markers of iPSC colonies by immunofluorescence (Additional file Figure 1B) and neural markers' expression by qPCR and immunofluorescence analysis of NSCs (Additional file Figure 1D–E respectively).

Antibodies

The primary antibodies used were as follows: OXPHOS (ab110413, Abcam), TOM20 (sc-11415, Santa Cruz), LC3 (B7931, Sigma for WB), LC3 (M152-3, MBL for immunostaining), pULK1 S757 (6888, Cell Signaling), p62 (610832, BD Bioscience), Ubiquitin (sc-8017, Santa Cruz), LAMP1 (sc-5570, Santa Cruz), TFEB (mbs120432, MyBioSource), Histone H3 (9715, Cell Signaling), GAPDH (ab8245, Abcam), Parkin (sc-32282, Santa Cruz), PINK1 (BC100-494, Novus), MTF2 (M6444, Sigma), OPA1 (612606, BD Bioscience), DLP1 (611113, BD Bioscience), Oct4 (09-0023, Stemgent), Nanog (4903, Cell Signaling Technologies), Sox2 (09-0024, Stemgent), SSEA4 (ab16287, Abcam), TRA 1-81 (09-0011, Stemgent), TRA 1-60 (09-0010, Stemgent), and Nestin (ab22035, Abcam). The secondary antibodies for immunoblot studies were horseradish peroxidase–conjugated anti-mouse (Jackson ImmunoResearch, West Grove, PA) or anti-rabbit (Thermo Fisher Scientific) and for immunofluorescence were anti-mouse or anti-rabbit Cyanine Cy2 or Cy3 labeled (Jackson ImmunoResearch) and anti-mouse or anti-rabbit Alexa Fluor 488 or 555 (Thermo Fisher Scientific).

Western Blot Analysis

The cells were lysed in RIPA buffer (Thermo Fisher Scientific) and centrifuged at 14,000 rpm at 4 °C for 10 min. Protein concentration was measured using Pierce™ BCA Protein Assay Kit (Thermo Fisher Scientific). Proteins were separated on 10 or 4–20% gradient Mini-PROTEAN TGX gels (BioRad) and transferred to nitrocellulose blotting membranes (BioRad). Western blot and immunoreactive proteins were developed using an enhanced chemiluminescence detection kit (BioRad).

Autophagy Flux Study

NSCs were treated with 10 μM carbonyl cyanide m-chlorophenylhydrazone (CCCP; C2759, Sigma-Aldrich) for 24 h followed by an additional treatment of PBS or Baf A1 (0.1 μM) for 4 h in the presence of CCCP [30]. After the treatment, cells were lysed in Western blot buffer and immunodetection of autophagy-involved proteins was performed as described. Quantification of the autophagy flux was analyzed according to autophagy standard guidelines [3, 47]. Briefly, autophagic vesicle synthesis was calculated as the ratio between the treatment with CCCP and Baf A1 with

respect to the condition without CCCP but maintaining Baf A1 treatment. Quantification of autophagic degradation ratio was obtained by the relation between the treatment with CCCP and Baf A1 and the ones without Baf A1 but maintaining CCCP treatment.

mtDNA Copy Number

DNA was isolated from cells with DNeasy Blood & Tissue Kit (69504, Qiagen). mtDNA content was assessed as described before [48] by quantification of a unique mitochondrial fragment relative to a single-copy region of the nuclear gene RNaseP. Quantitative PCR was performed in a QuantStudio 6 Flex Real-Time PCR System (Applied Biosystems) by using Thermo Scientific Maxima SYBR Green/Rox qPCR Master Mix (K0222, Thermo Scientific). mtDNA fragment was amplified using the following primers: Mito-F: CACTTTCC ACACAGACATCA and Mito-R: TGGTTAGGCTGGTG TTAGGG. Nuclear content was amplified using the following primers: RNaseP-F: CCCCGTTCTCTGGGAACTC and RNaseP-R: TGTATGAGACCACTCTTTCCCATA.

Complex I Activity Measurement

The NADH:HAR (hexaammineruthenium (III)) oxidoreductase activity of complex I [49] was determined spectrophotometrically using a plate reader (SpectraMax M5, Molecular Devices, USA). Oxidation of 0.160 mM NADH ($\varepsilon_{346\ nm}$ 6.22 mM^{-1} cm^{-1}) by 1 mM HAR was followed at 346 nm in 0.2 mL of KCl-Tween standard buffer (KCl 125 mM, HEPES 20 mM, $MgCl_2$ 1 mL/L, 0.5 mL/L Tween 20; pH 7.8) supplemented with 40 μg/mL alamethicin (to permeabilize mitochondria), 1 mM $MgCl_2$, 1 mM cyanide, and 30 μg protein/mL mitochondria.

Isolation of Nuclear and Cytoplasmic Extract

The nuclear extraction was prepared using an NE-PER Nuclear Cytoplasmic Extraction Reagent kit (78833, Thermo Fisher Scientific) according to the manufacturer's instruction. Briefly, the treated cells were washed twice with cold PBS and centrifuged at 500*g* for 3 min. The cell pellet was suspended in 200 μL of cytoplasmic extraction reagent I by vortexing. The suspension was incubated on ice for 10 min followed by the addition of 11 μL of a second cytoplasmic extraction reagent II, vortexed for 5 s, incubated on ice for 1 min, and centrifuged for 5 min at 16,000*g*. The supernatant fraction (cytoplasmic extract) was transferred to a pre-chilled tube. The insoluble pellet fraction, which contains crude nuclei, was resuspended in 100 μL of nuclear extraction reagent by vortexing during 15 s and incubated on ice for 10 min, then centrifuged for 10 min at 16,000*g*. The resulting supernatant, constituting the nuclear extract, was used for the subsequent experiments.

Immunocytochemistry

NSCs were grown on sterile glass coverslips, treated as described for each experiment, followed by washing with PBS and fixing with 4% paraformaldehyde in PBS for 20 min at room temperature. After blocking with PBS containing 1% BSA and permeabilizing with 0.1% Triton X-100 and glycine 1 M for 30 min, cells were washed with PBS and stained by indirect immunofluorescence using the antibodies described before. Samples were mounted with ProLong Gold Antifade (P-36930, Life Technologies), and randomly chosen field images were obtained in an Inverted Confocal DMI6000CS (Leica, Wetzlar, Germany) fluorescence microscope.

Quantification of Colocalization and Vesicle Average Size

Colocalization analysis was performed with ImageJ software (Bethesda, MD, USA) as it was previously described [30]. Briefly, by a threshold intensity, binary images were obtained and Image Calculator tool was used to generate an image harboring only overlapping structures. Colocalization measurement was obtained by quantifying the area occupied by the overlapping elements per cell. At least 200 cells were measured for each cell line. For the lysosomal size analysis, cells were thresholded and the average size was calculated using the particle analyzer of the ImageJ software.

Mitochondrial Morphology Study

Cells were fixed with 4% paraformaldehyde and mitochondrial pattern was observed by TOM20 staining. Images were acquired with Inverted Confocal DMI6000CS (Leica, Wetzlar, Germany) fluorescence microscope. For analysis, we used the Mitochondrial Network Analysis [3] toolset, a combination of different ImageJ macros that allows the semi-automated analysis of mitochondrial networks in cultured mammalian cells [30]. Briefly, the image was converted to binary by thresholding following the conversion to a skeleton that represents the features in the original image using a wireframe of lines one pixel wide. All pixels within a skeleton were then grouped into three categories: end point pixels, slab pixels, and junction pixels. The plugin analyzes how the pixels are spatially related and defined to measure the length of each branch and the number of branches in each skeletonized feature as well as the mitochondrial network morphology. The parameters used in the study were as follows: (1) individuals, punctate, rods, and large/round mitochondrial structures; (2) networks, mitochondrial structures with at least a single node and three branches; (3) the mean number of branches per network; and (4) the average of length of rods/branches. One hundred cells per each independent experiment were used to quantify the pattern of mitochondria.

Quantitative Real-time PCR Assays

RNA was isolated by using SV Total RNA Isolation System (Promega, Madison, WI, USA) following provider's guidelines. RNA was reverse transcribed into cDNA using ImProm-II reverse transcription systems (Promega, Madison, WI, USA), which was then amplified by quantitative PCR performed in a QuantStudio 6 Flex Real-Time PCR System (Applied Biosystems) by using Thermo Scientific Maxima SYBR Green/Rox qPCR Master Mix (K0222, Thermo Scientific). The primers used for the detection were TFEB-F: CCAGAAGCGAGAGCTCACAGAT, TFEB-R: TGTGATTGTCTTTCTTCTGCCG, LC3-F: GAGAAGCA GCTTCCTGTTCTGG, LC3-R: GTGTCCGTTCACCA ACAGGAAG, LAMP1-F: ACGTTACAGCGTCC AGCTCAT, LAMP1-R: TCTTTGGAGCTCGCATTGG, SOX1-F: GCGGAAAGCGTTTTCTTG, SOX1-R: TAATCTGACTTCTCCTCCC, SOX2: ATGCACCG CTACGACGTGA, SOX2-R: CTTTTGCACCCCTC CCATTT, Nestin-F: CAGCGTTGGAACAGAGGTTGG, and Nestin-R: TGGCACAGGTGTCTCAAGGGTAG. Gene expressions were normalized to human GAPDH using the primers GAPDH-F: GTCGGAGTCAACGGATT and GAPDH-R: AAGCTTCCCGTTCTCAG.

Statistical Analysis

Graphs represent means and standard errors of the values obtained from, at least, experimental triplicates using control and PS1 M146L samples, which are specified in each legend to the figure. When necessary, values represented in the graphs were obtained by normalizing every PS1 M146L sample data with the correspondent control sample. Student's *t* test was performed for statistical comparison of the data sets. To examine the differences between experimental factors and their interaction, a two-way analysis of variance (ANOVA) test was performed. When more than two experimental groups were compared, a post hoc Bonferroni test was used. Non-parametric Mann–Whitney *U* test was used when the distribution of the data was not normal. The differences are given with their corresponding statistical significance or *p* value, which is the probability that the difference occurred merely by chance under the null hypothesis.

Availability of Data and Materials

A detailed description of "Methods" and all the data reported in this study are included in the manuscript. The original cell lines used in the study are available to other researchers from a commercial entity (Coriell Institution), and the hiPSCs derived from these cell lines are available to other researches upon approval of a Material Transfer Agreement between them and NYSCF.

Results

Mitochondrial Anomalies in PS1 M146L NSCs

Although, previous results demonstrate mitochondrial dysfunction and oxidative stress in human NSCs related to Aβ pathology [50], further investigations are needed to understand the involvement of mitochondrial anomalies in the pathogenesis of AD. We elected to use a PS1 M146L homozygous knockin model for our study (see "Methods" for TALEN-mediated generation), as this would facilitate more robust AD phenotypes while still keeping PS1 under physiological expression and allowing cross comparisons with the isogenic control backbone (Additional file Figure 1). Thus, we first assayed the expression levels of the oxidative phosphorylation–related proteins (OXPHOS) by immunoblot. Decreased expression levels were detected for the subunits of ATP synthase (complex V), cytochrome c oxidase (complex IV), cytochrome c reductase (complex III), succinate dehydrogenase (complex II), and NADH:CoQ reductase (complex I) OXPHOS complexes in PS1 M146L NSCs, as compared with control cells (Fig. 1a–b). A downregulation of expression of mitochondrial complex I subunits had been described in brains of early and severe AD patients [51], as well as a decrease in complex I activity in several AD mouse models [52]. Therefore, we analyzed the activity of complex I [53, 54] in our model and found that it was decreased in PS1 M146L NSCs (Fig. 1c). Moreover, we observed that mitochondrial DNA (mtDNA) copy number in PS1 M146L NSCs was significantly increased as compared with the control cells (Fig. 1d). In parallel, PS1 M146L cells exhibited higher levels of TOM20, a constitutive mitochondrial marker (Fig. 1e). One of the reasons to this mitochondrial accumulation could be a failure in the recycling process of mitochondria.

Impaired Autophagy in PS1 M146L NSCs

The transcription factor EB (TFEB) is a master regulator of transcription of target genes involved in autophagy and lysosome biogenesis [55]. To identify whether autophagy may be altered in our PS1 M146L NSCs, we analyzed the expression of autophagy-related markers measured by RT-qPCR. PS1 M146L cells exhibited a decreased TFEB expression and a reduction in the expression of the autophagy marker LC3 and the lysosomal marker LAMP1 (Fig. 2a). Then, we analyzed the TFEB protein levels under basal conditions in the whole lysate, and we observed a significant decreased in PS1 M146L NSCs compared with control cells (Additional file Figure 2A). Due to the cellular localization and activity of TFEB are mainly controlled by its phosphorylation status [56], we studied the TFEB subcellular localization in control and PS1 M146L NSCs by the isolation of cytosolic and nuclear fraction. The results

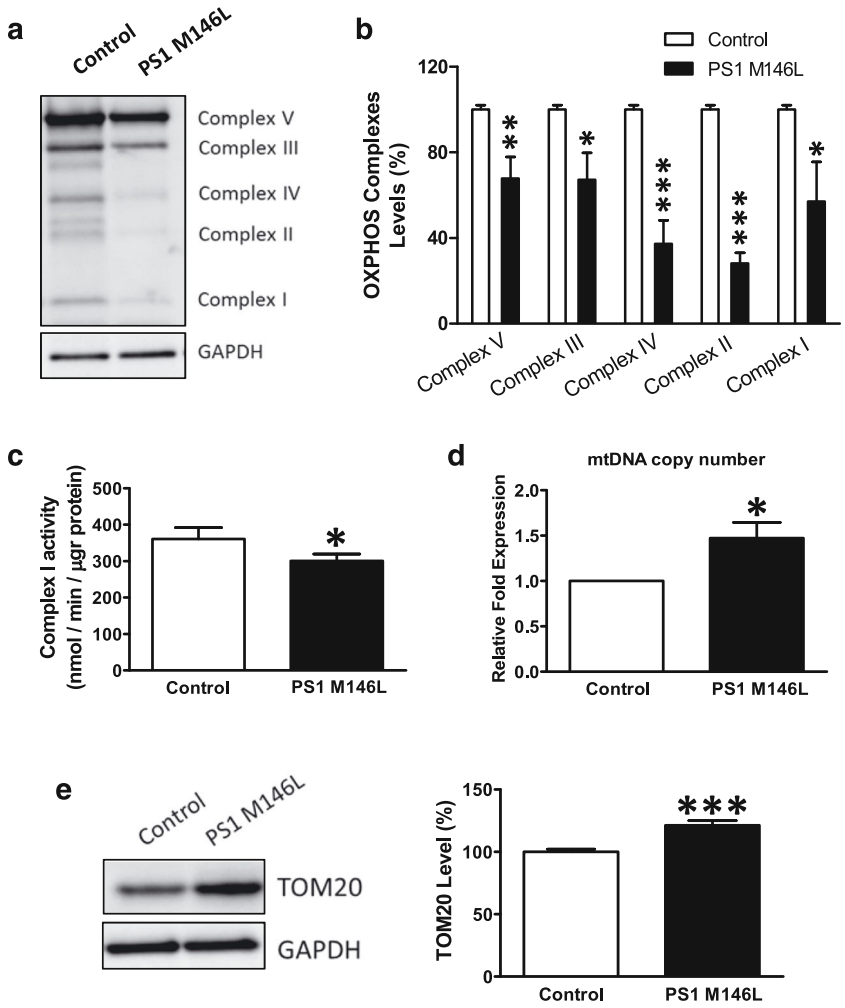

Fig. 1 Mitochondrial anomalies in PS1 M146L NSCs. **a**, **b** Representative immunoblot and quantification of mitochondrial OXPHOS respiratory complex protein levels under basal conditions. **c** Complex I NADH:hexaammineruthenium (HAR) reductase activities were determined spectrophotometrically in whole cell homogenates as described in "Methods." **d** Expression levels of mtDNA copy number by qPCR of a unique mitochondrial DNA fragment relatively to a single-copy region of the nuclear gene RNaseP. **e** Representative immunoblot of TOM20 protein levels of cells incubated in the presence of CCCP (10 μM) for 24 h. Quantification of TOM20 expression under basal conditions. Graphs showed means and SEM ($n = 5$ independent experiments; $^{*}p < 0.05$; $^{**}p < 0.01$; $^{***}p < 0.001$)

showed that TFEB localizes predominantly in the cytoplasm of PS1 M146L NSCs suggesting that a substantial fraction of TFEB is phosphorylated correlating with a reduction of dephosphorylation and activation of TFEB monitored by its significant decreased translocation to the nuclear compartment under basal conditions (Additional file Figure 2b). To determine autophagy flux, NSCs were treated with CCCP followed by a treatment of Baf A1 in the presence of CCCP to block the degradation phase of autophagy. Immunoblot analysis revealed a significantly decreased amount of autophagic vesicles (AVs) in PS1 M146L cells exhibiting a decrease in LC3II protein levels and a decreased LC3II/LC3I ratio (Fig. 2b, c) under basal conditions. Although CCCP treatment showed induction of AVs, a reduction of autophagosome synthesis in PS1 M146L cells was observed. This observation correlates with significantly smaller LC3II accumulation compared with control samples after CCCP treatment when vacuole degradation was blocked by Baf A1 (Fig. 2d). Moreover, we observed a decreased degradation of AVs in PS1 M146L NSCs (Fig. 2e), suggesting a decreased autophagy flux stemming from a deficient autophagic vacuole formation. This data correlates with the significant increase in phosphorylated ULK1 at Ser758 levels in PS1 M146L NSCs (Fig. 2f). The ULK1 kinase is the key initiator of the autophagic process in mammalian cells, and its phosphorylation inactivates the kinase resulting in autophagy downregulation [57]. To confirm this hypothesis, we examined the turnover of p62, an adaptor protein that is degraded by autophagy, under the same conditions. We observed that basal levels of p62 were notably elevated in PS1 M146L cells compared with control samples (Fig. 2g, h) as had been previously reported [58]. Moreover, these cells exhibited a remarkably lower degradation of p62 (Fig. 2i). Similar to p62, other autophagy adaptors such as optineurin (OPTN) and NDP52 also directly bind ubiquitin and LC3 to coordinate the autophagosome-mediated engulfment of cargo [59]. We found that levels of OPTN were increased, and levels of NDP52 were not altered in PS1 M146L NSCs as compared with control cells (Additional file Figure 2B–C). Consistent with these autophagy alterations, we also detected a significant

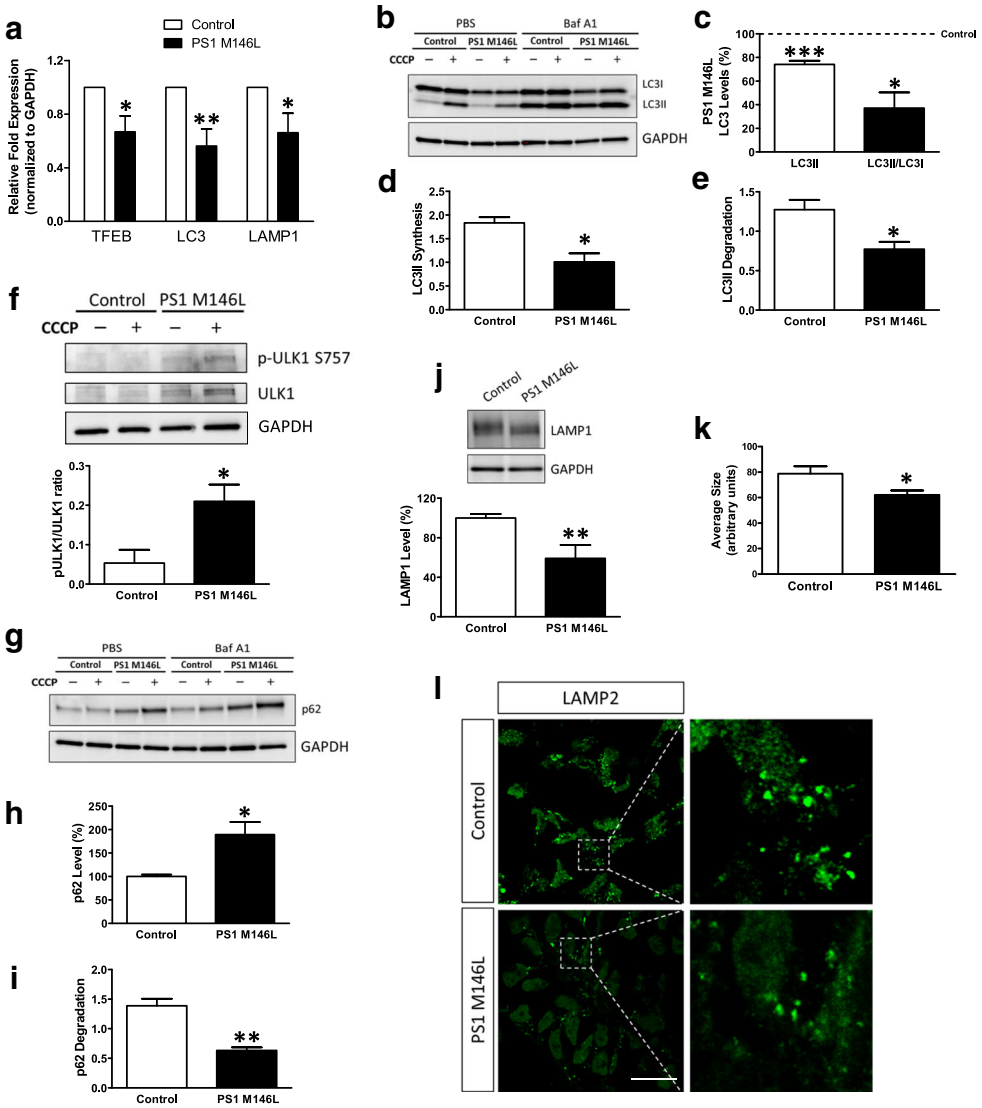

Fig. 2 Autophagy failure in PS1 M146L NSCs. **a** Expression levels of TFEB, LC3, and LAMP1 measured by RT-qPCR in control and PS1 M146L NSCs under basal conditions. Results were normalized to GAPDH and are presented relative to control. **b** Representative immunoblot of LC3 expression for the study of autophagy flux. NSCs were treated with 10 μM CCCP for 24 h followed by an additional treatment of PBS or Baf A1 (0.1 μM) for 4 h in the presence of CCCP. **c** Quantification of LC3II levels and LC3II/LC3I ratio in the PS1 M146L samples with respect to the controls under basal conditions. **d** Quantification of LC3II synthesis as the ratio between the treatment with CCCP and Baf A1 with respect to the condition without CCCP but maintaining Baf A1 treatment. **e** Quantification of autophagic degradation ratio was obtained by the relation between the treatment with CCCP and Baf A1 and the ones without Baf A1 but maintaining CCCP treatment. **f** Representative immunoblot and quantification of pULK1 S757 expression treated with CCCP (10 μM) for 24 h. **g**, **h** Representative immunoblot of p62 expression after the treatment as in **b** and quantification of basal levels. **i** Quantification of p62 degradation ratio as defined in **e**. **j** Representative immunoblot and quantification of LAMP1 under basal conditions. **k**, **l** Representative confocal microscopy immunofluorescence images showing the lysosomal marker LAMP2 and quantification of lysosomal average size of control and PS1 M146L NSCs in basal conditions. Images on the right show enlargement of the squared area. Graphs showed means and SEM ($n = 5$ independent experiments; $^{*}p < 0.05$; $^{**}p < 0.01$). Scale bar 20 μm

accumulation of ubiquitinated proteins in PS1 M146L cells (Additional file Figure 1D). To address a possible lysosomal dysfunction, we studied the levels of lysosomal markers in PS1 M146L NSCs. We observed a decrease in the levels of LAMP1 (Fig. 2j) in parallel with a clear reduction in the average size of lysosomes in PS1 M146L cells, as compared with control cells (Fig. 2k, l).

Mitophagy Alterations in PS1 M146L NSCs

The obtained data indicate a defect in autophagy in PS1 M146L NSCs. Hence, we investigated whether mitochondrial recycling could be deregulated by the *PS1* mutation. PS1 M146L cells showed elevated levels of Parkin protein (Fig. 3a). On the other hand, PINK1 protein levels were highly

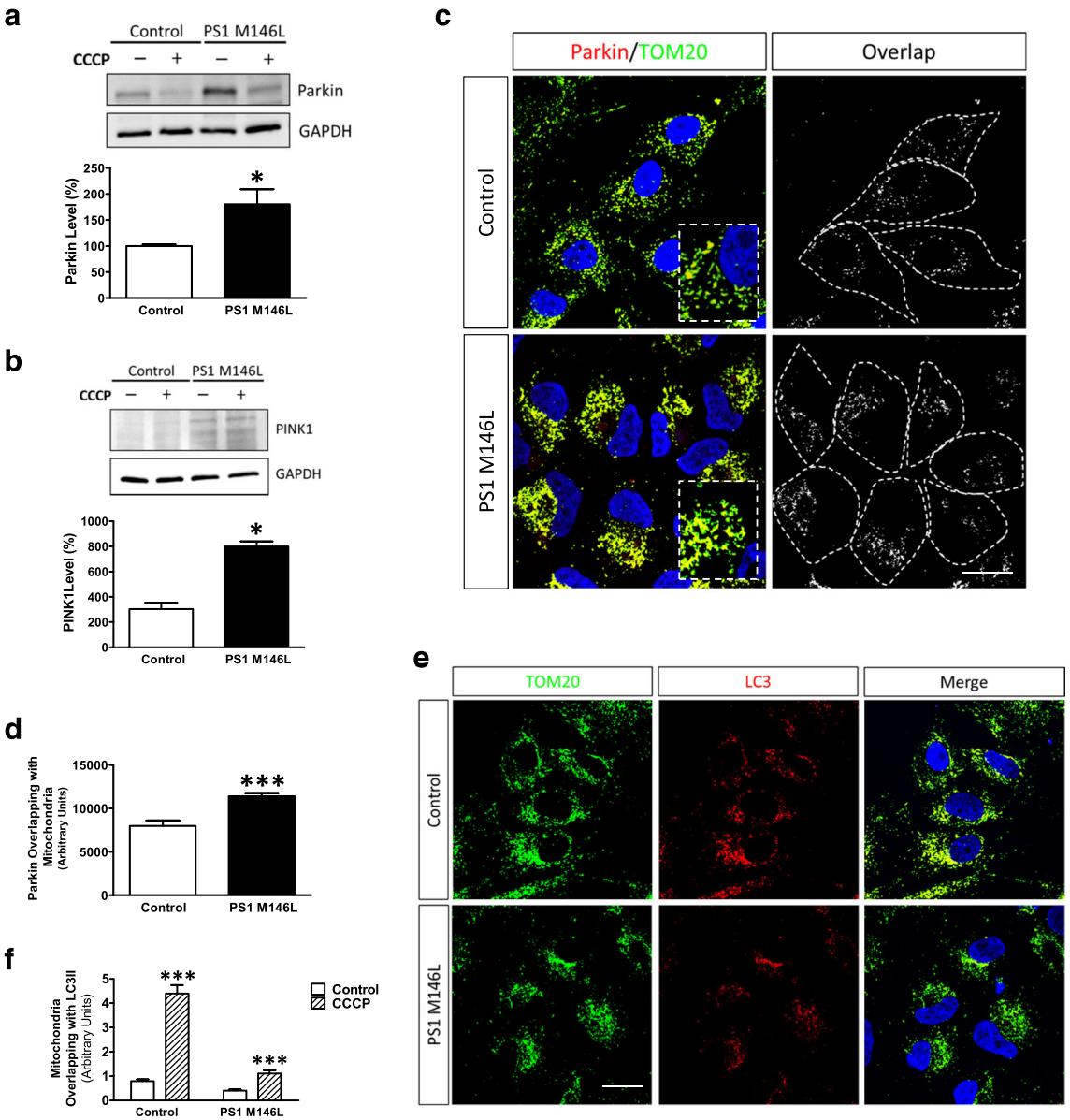

Fig. 3 Mitophagy impairment in PS1 M146L NSCs. **a** Representative immunoblot and quantification of Parkin levels under basal conditions. **b** Representative immunoblot and quantification of PINK1 levels in control and PS1 M146L NSCs treated with CCCP (10 μM) for 24 h. **c**, **d** Representative confocal microscopy immunofluorescence images showing Parkin in red and TOM20 as a mitochondrial constitutive marker in green in the same cells treated with CCCP (10 μM) for 1 h. On the right, binary image represents the colocalization of both labels and dotted line delimits cytoplasm of each cell. **e** Representative confocal microscopy immunofluorescence images showing LC3 in red and TOMM20 in green of control and PS1 M146L NSCs treated with CCCP (10 μM) for 24 h. **f** Quantification of the colocalization between LC3 and TOMM20 expressed as area occupied by the overlapping elements per cell. Graphs showed means and SEM ($n = 5$ independent experiments; $^{*}p < 0.05$; $^{***}p < 0.001$). Scale bar 20 μm

increased in PS1 M146L NSCs compared with the controls, after the treatment with CCCP for 24 h (Fig. 3b). Parkin is recruited to impaired mitochondria with low membrane potential in mammalian cells and promotes the engulfment of mitochondria by autophagosomes and the selective elimination of impaired mitochondria [60]. Thus, we studied the recruitment of Parkin to the mitochondria by immunofluorescence after the treatment with CCCP for 1 h (Fig. 3c). We observed that mitochondrial localization of Parkin was increased in PS1 M146L cells (Fig. 3d) correlating with a decreased ubiquitin phosphorylation at Ser65 and Parkin activation (Additional file Figure 3), suggesting an accumulation of damaged mitochondria that cannot be recycled by mitophagy. Accordingly, we found a reduction of mitochondrial content in autophagic vesicles after CCCP treatment, as indicated by a decrease in colocalization of TOM20 and LC3II (Fig. 3e, f). Overall, these data suggest mitophagy impairment due to autophagy blockage.

Changes in Mitochondrial Dynamics in PS1 M146L NSCs

Mitochondrial dynamics is regulated by a machinery involving large dynamin-related GTPases with mitofusin 1 (MFN1), mitofusin 2 (MFN2), and optic atrophy 1 (OPA1) proteins being involved in mitochondrial fusion [61]. Mitochondrial fission is mediated by dynamin-like protein 1 (DLP1) through its interaction with four mitochondrial receptor proteins [61–63]. Previous studies revealed an impaired balance of mitochondrial fission and fusion proteins in brains of AD patients [64]. Therefore, we examined whether proteins that control mitochondrial dynamics could be altered in PS1 M146L NSCs. We observed diminished levels of fusion protein MTF2 and OPA1 in PS1 M146L cells (Fig. 4a, b). Several studies demonstrated reduced levels of DLP1 in neurons and fibroblasts obtained from AD patients [65, 66]. We observed a decrease in DLP1 fission protein level in PS1 M146L cells (Fig. 4c). DLP1 function depends on its subcellular localization [67]; therefore, we studied its distribution by immunofluorescence analysis of mitochondria labeled with TOM20. Quantitative analysis revealed an increase in DLP1 abundance in mitochondria in PS1 M146L NSCs, as compared with control cells (Fig. 4d). An aberrant mitochondrial morphology and distribution in AD had been reported earlier [65]. These data and the previously reported downregulation of mitochondrial dynamics proteins prompted us to evaluate morphological features of mitochondria. We examined the mitochondrial network skeleton in representative images of control and PS1 M146L NSCs. The network parameters were calculated by the Mitochondrial Network Analysis toolset [68] (Fig. 4e). Although there were no differences in the number of individual puncta and rod mitochondrial structures (Fig. 4f) and networks (mitochondrial structures with at least a single node and three branches, Fig. 4g) between control and PS1 M146L cells, we observed a remarkably diminished amount of the branches per network and the shorter length of the branches in PS1 M146L NSCs (Fig. 4h, i), which correlated with an increase in the number of fragmented mitochondria, likely as a consequence of excessive mitochondrial fission.

Bexarotene Treatment Compensates Autophagy Deficiency and Restores Mitophagy

Recent studies have demonstrated neuroprotective potential of bexarotene in different neurodegenerative diseases including AD [37, 38, 40]. To evaluate whether bexarotene treatment of PS1 M146L NSCs promotes autophagy activation, we measured the RNA expression of autophagy-related markers TFEB, LC3, and LAMP1. We found that bexarotene-treated cells demonstrate an induced expression of these autophagy target genes (Fig. 5a). Moreover, the autophagy flux study revealed a diminished AV content (Fig. 5b, c) correlating with an increased autophagosome synthesis and degradation in PS1 M146L cells (Fig. 5d, e; previously decreased in PS1 mutant cells (Fig. 2d, e)) due to an autophagy induction after the treatment with bexarotene. These data correlate with a reduction in p62 accumulation caused by p62 degradation induction (Fig. 5f–h; previously increased in PS1 mutant cells (Fig. 2h)) as well as with an increase in LAMP1 protein abundance (Fig. 5i) in PS1 M146L cells after the treatment. Together, these data suggest that bexarotene activates the autophagy flux.

Further, we examined whether the bexarotene treatment improves the mitochondrial recycling process. We observed that Parkin levels remained increased in PS1 M146L cells (Fig. 6a), and its targeting to mitochondria after CCCP insult and bexarotene treatment was not disturbed (Fig. 6b). Finally, bexarotene-treated PS1 M146L cells demonstrated an enhanced mitophagy, as can be judged from increased ubiquitin phosphorylation at Ser65 and Parkin activation (Fig. 6c. As a result, mitochondrial recycling was increased, which was reflected by a decrease in the mtDNA copy number as well as the levels of TOM20 in bexarotene-treated cells (Fig. 6d, e). On the other hand, the treatment with bexarotene recovered the protein levels of the oxidative phosphorylation system complex I as well as its activity suggesting an improvement of the respiratory chain function (Fig. 6f, g).

Bexarotene Treatment Rescues Altered Mitochondrial Network Morphology

Next, we examined whether bexarotene treatment could improve the mitochondrial morphology. First, we analyzed the mitochondrial dynamics protein levels in bexarotene-treated PS1 M146L cells. We found that MTFN2, OPA1, and DLP1 levels were restored to the levels observed in control cells (Fig. 7a–c). In order to analyze whether these changes could reflect a recovery of the mitochondrial morphology, we examined the mitochondrial network skeleton by MiNa after the treatment with bexarotene (Fig. 7d). The treatment increased the length of the branches in PS1 M146L cells (Fig. 7f–i). These data strongly suggest that bexarotene treatment rescued mitochondrial network morphology and distribution.

Discussion

Large numbers of PS1/PS2 mutations are linked to FAD [69]. These PS1/PS2 mutations compromise the essential physiological roles of presenilin in memory, synaptic function, and neuronal survival, eventually leading to neurodegeneration and dementia [70, 71]. Prior studies of AD pathogenesis had been focused on the degeneration of existing neuronal circuits. However, deciphering the physiological state of NSCs is the key for understanding AD development. It was shown that physiological levels of expression of a single *PS1* M146V

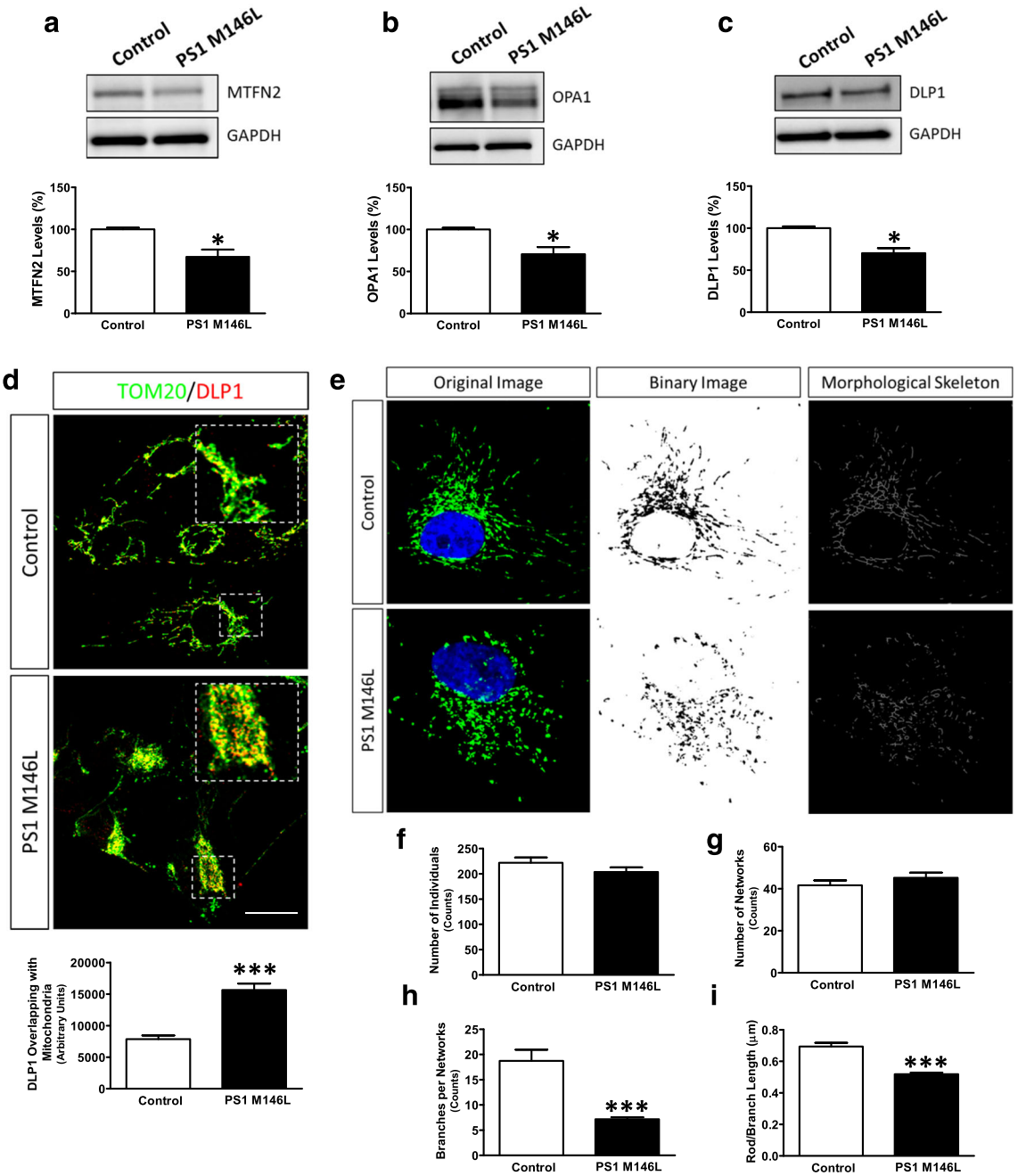

Fig. 4 Alterations in mitochondrial network morphology in PS1 M146L NSCs. Representative immunoblots and quantification of mitochondrial dynamics proteins **a** MTFN2 and **b** OPA1 and **c** DLP1 under basal conditions. **d** Representative confocal microscopy immunofluorescence images showing DLP1 in red and TOM20 in green and colocalization quantification of control and PS1 M146L NSCs under basal conditions. **e** Representative images showing mitochondrial morphological skeleton generated by Mitochondrial Network Analysis [3] toolset of control and PS1 M146L NSCs under basal conditions. Quantification of **f** number of individuals, **g** number of networks, **h** branches per network, or **i** length of the branches. Graphs showed means and SEM ($n = 3$ independent experiments; $^{*}p < 0.05$; $^{***}p < 0.001$). Scale bar 20 µm

allele are sufficient to impair environmental enrichment-induced adult hippocampal NSC proliferation, survival, and neuronal differentiation, in vivo [72]. The *PS1* M146L mutation is a prevalent and most characterized FAD mutation that shows typical phenotypes of AD [73–75]. It appears that PS1-mutated isogenic hiPSC-derived NSC that we employed in this study is a useful tool to examine the alterations in FAD progenitors because it is a consistent and fully controllable cell model relevant to the study of AD with the benefit to proliferate the cells in the amounts sufficient for a screening of new drugs.

In the present work, we have analyzed the mitochondrial recycling process in a human neural cell model, generated from iPSC harboring the *PS1* M146L mutation. We have

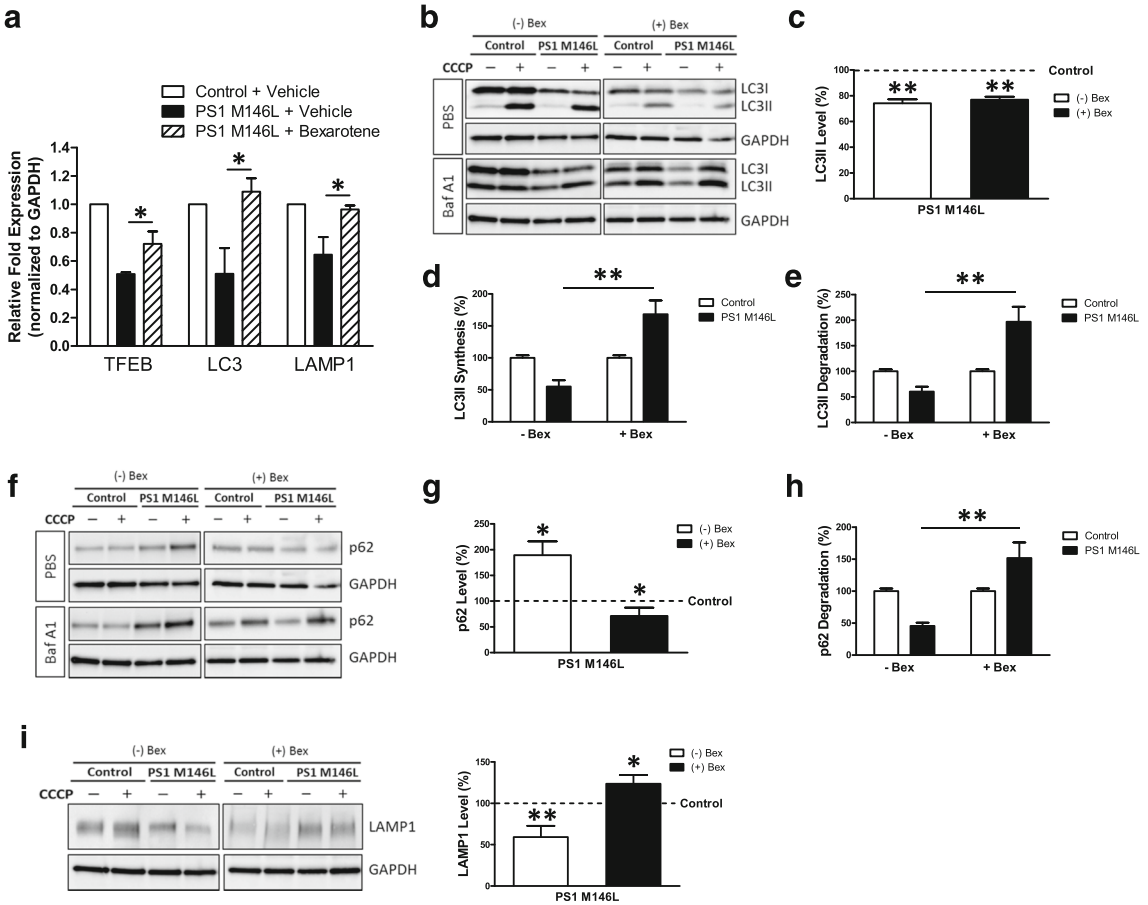

Fig. 5 Autophagy induction in PS1 M146 L cells after bexarotene treatment. **a** Expression levels of TFEB, LC3, and LAMP1 measured by RT-qPCR in control and PS1 M146L NSCs after the treatment with bexarotene (0.5 μM) for 24 h. **b** Representative immunoblot of LC3 expression for the study of autophagy flux after the treatment with bexarotene. After the treatment with bexarotene (0.5 μM) for 24 h, NSCs were treated with 10 μM CCCP for 24 h followed by an additional treatment of PBS or Baf A1 (0.1 μM) for 4 h in the presence of CCCP. **c** Quantification of LC3II basal levels in the PS1 M146L samples with respect to the controls before and after bexarotene treatment. **d** Quantification of LC3II synthesis as the ratio between the treatment with CCCP and Baf A1 with respect to the condition without CCCP but maintaining Baf A1 treatment. **e** Quantification of autophagic degradation ratio was obtained by the relation between the treatment with CCCP and Baf A1 and the ones without Baf A1 but maintaining CCCP treatment. **f** Representative immunoblot of p62 expression after the treatment as in **b** and **g** quantification of basal levels before and after bexarotene treatment. **h** Quantification of p62 degradation ratio as defined in **e**. **i** Representative immunoblot and quantification of LAMP1 basal levels before and after the treatment with bexarotene. Graphs showed means and SEM ($n = 5$ independent experiments; $^{*}p < 0.05$; $^{**}p < 0.01$)

demonstrated a deregulation of autophagy as a result of a deficiency in autophagy induction which is manifested by the decreased expression of autophagy-related markers, such as TFEB expression and its nuclear translocation, as well as lower levels of autophagic vesicle (LC3) formation (Fig. 2a–e). This data correlates with the accumulation of ubiquitinated proteins and the proteins degraded by autophagy (p62) (Fig. 2g, h). Earlier, an accumulation of p62 has been observed in neuronal and glial ubiquitin-containing inclusions [76] as well as in neurofibrillary tangles [77] in AD brains. We also found lysosomal anomalies in PS1 M146L NSCs manifested by an abnormally decreased size of lysosomes (Fig. 2k, l). This data is in line with previous findings where lysosomal function was compromised by a deficit in lysosomal acidification [58]. In that study, PS1 was demonstrated to act as a chaperone protein that facilitates the N-glycosylation of V-ATPase subunit V0a1, which helps V-ATPase traffic to lysosome and complete lysosome acidification. These results combined with the reduced expression of subunits of respiratory chain complexes and ATP synthase as well as reduced activity of complex I in PS1 M146L cells correlates with recent report where chronic mitochondrial respiratory chain dysfunction results in a repression of TFEB/MITF transcriptional activity and lysosomal biogenesis [78]. Overall, these data suggested that PS1 mutation blocks autophagy induction in PS1 M146L NSCs. The data obtained in our study confirms this hypothesis.

Our findings also demonstrated that mitophagy triggered by mitochondrial insult is severely affected resulting in mitochondrial accumulation in our PS1 M146L cells (Fig. 1d, e). These cells showed a marked accumulation of Parkin and

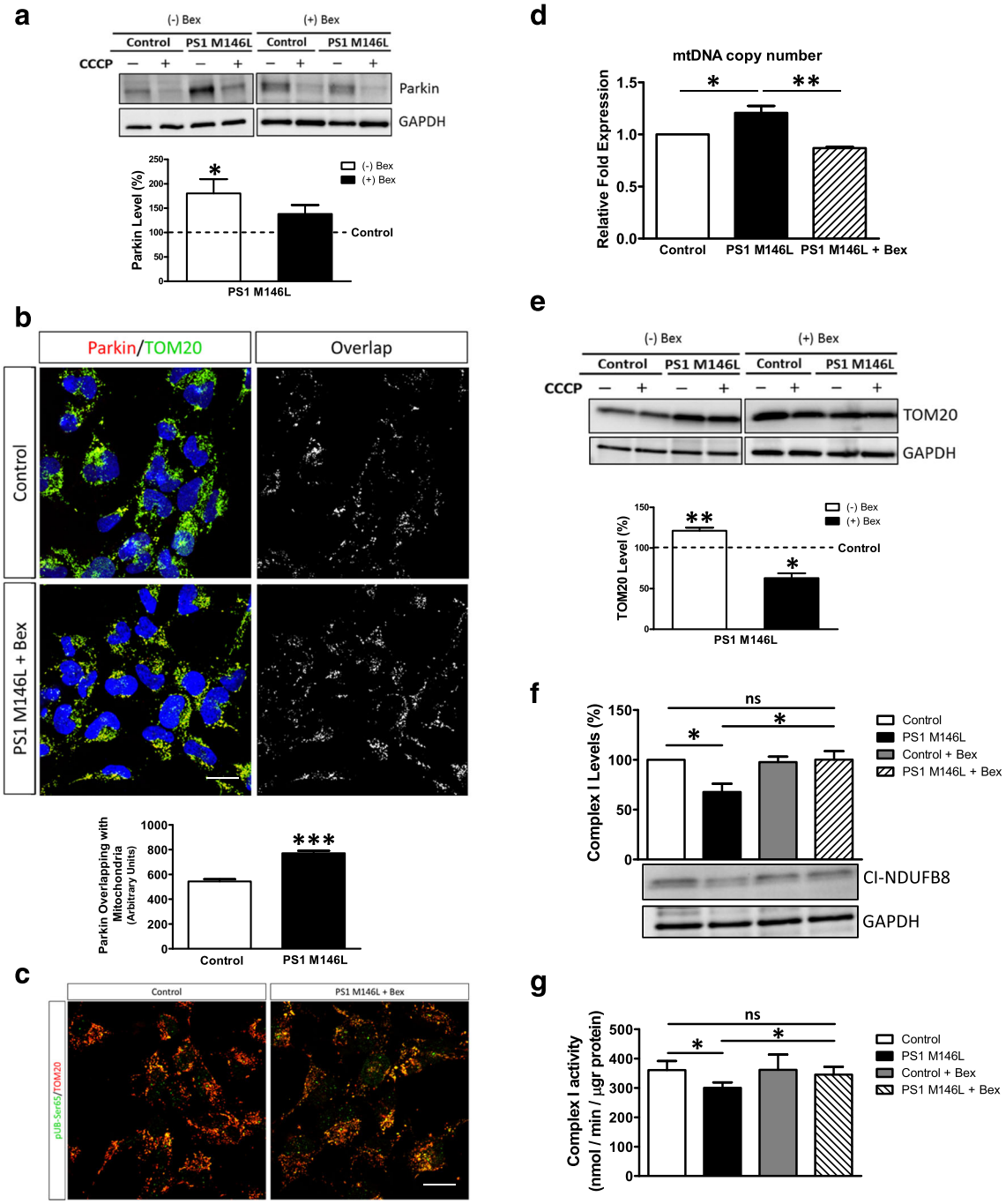

Fig. 6 Bexarotene treatment compensates mitophagy deficiency in PS1 M146L cells. **a** Representative immunoblot and quantification of Parkin basal levels after the treatment with bexarotene. **b** Representative confocal microscopy immunofluorescence images showing Parkin in red and TOM20 as a mitochondrial constitutive marker in green in control and PS1 M146L cells treated with bexarotene (0.5 μM) for 24 h followed by an additional treatment of CCCP (10 μM) for 1 h. On the right, binary image represents the colocalization of both labels and dotted line delimits cytoplasm of each cell. **c** Representative confocal microscopy immunofluorescence images showing pUB-Ser65 in green and TOM20 in red in control and PS1 M146L cells treated with bexarotene (0.5 μM) for 24 h followed by an additional treatment of CCCP (10 μM) for 1 h. **d** Expression levels of mtDNA copy number by RT-qPCR of a unique mitochondrial DNA fragment relatively to a single-copy region of the nuclear gene RNaseP after the treatment with bexarotene. **e** Representative immunoblot and quantification of TOM20 basal levels after the treatment with bexarotene. **f** Representative immunoblot image and quantification of complex I protein levels after the treatment with bexarotene. **g** Complex I NADH:hexaammineruthenium (HAR) reductase activities were determined spectrophotometrically in whole cell homogenates after the treatment of bexarotene for 24 h as described in "Methods." Graphs showed means and SEM ($n = 5$ independent experiments; $^{*}p < 0.01$, $^{**}p < 0.01$; $^{***}p < 0.001$). Scale bar 20 μm

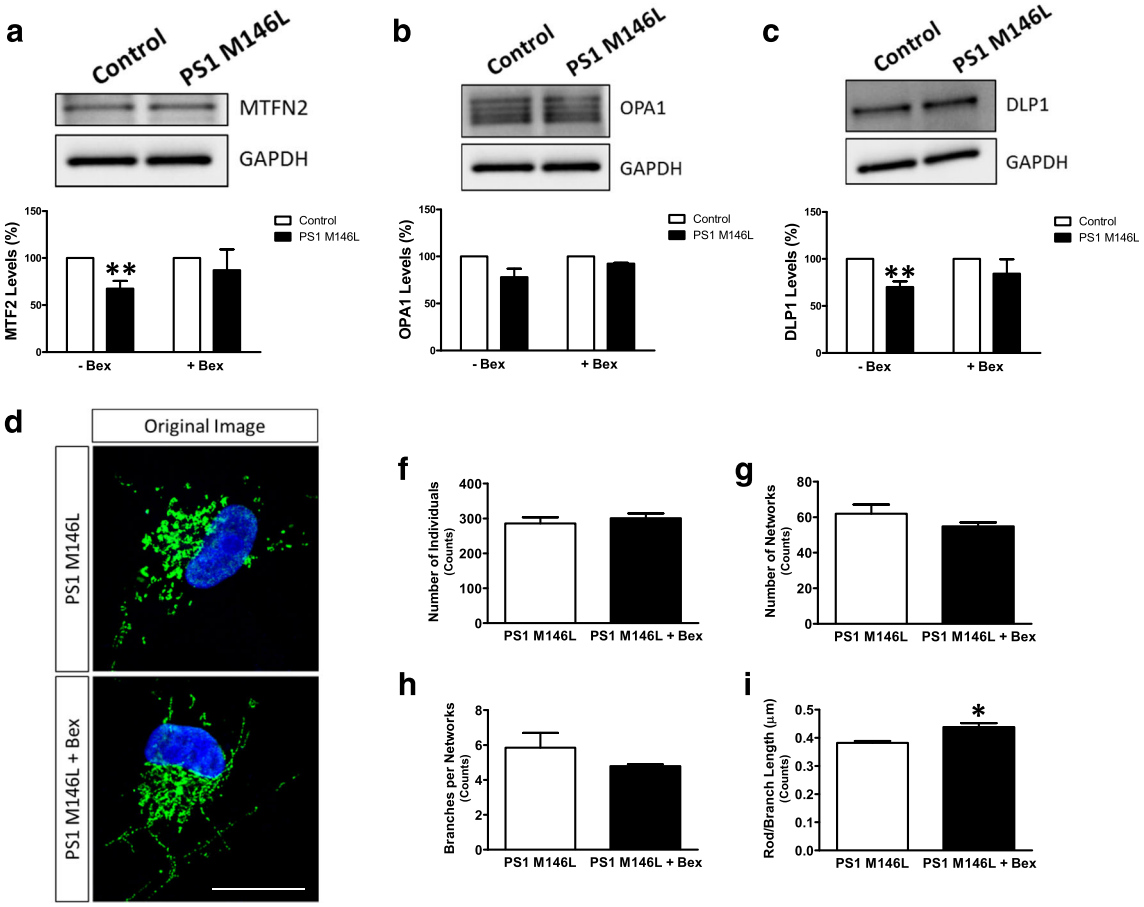

Fig. 7 Mitochondrial morphology restoration in PS1 M146L NSCs after bexarotene treatment [3]. Representative immunoblots and quantification of mitochondrial dynamics proteins **a** MTFN2 and **b** OPA1 and **c** DLP1 levels after the treatment with bexarotene. **d** Representative images showing mitochondrial morphological skeleton generated by MiNa toolset of control and PS1 M146L NSCs after the treatment with bexarotene. Analysis of **f** number of individuals, **g** number of networks, **h** branches per network, or **i** length of the branches. Graphs showed means and SEM ($n = 5$ independent experiments; $*p < 0.05$; $**p < 0.01$). Scale bar 20 μm

PINK1 (Fig. 3a, b). This had been previously attributed to an accumulation of depolarized mitochondria unable to be degraded by autophagy [25, 79]. The Parkin accumulation that we have observed in PS1 mutant cells is in line with earlier reports demonstrating that an accumulation of insoluble Parkin, intraneuronal Aβ, and phospho-MAPT was detected in AD brain autophagosomes, indicating autophagy failure [80]. Additionally, the upregulation of Parkin expression had been suggested to serve as a defense mechanism counteracting AD-associated stress-induced damage [81]. Further, upon mitochondrial depolarization, Parkin (despite its correct translocation to the mitochondria) does not correctly activate and properly target mitochondria to autophagic vesicles, correlating with the autophagy blockage in PS1 M146L NSCs. To note, our finding agrees well with published results obtained with 5xFAD mice exhibiting drastically increased, age-dependent Parkin translocation to synaptosomal mitochondria [82]. More recently, Bohr's group showed alterations in mitochondrial function and changes in the immunoreactivity of mitophagy-associated proteins in both brain biopsies and iPSC-derived neurons from FAD AD patients [83]. They also showed that Aβ inhibits mitophagy while mitophagy induction reduces Aβ in the hippocampus of transgenic APP/PS1 AD mice. In correlation with our findings, the authors suggested an impaired initiation of selective mitochondrial autophagy, due to decreased levels of activated mitophagic proteins, resulting in the accumulation of dysfunctional mitochondria and impaired cellular energy metabolism. They demonstrated that defective mitophagy, which can be caused by both Aβ and p-tau, is a major element of AD progression and memory loss in a manner that is conserved from *C. elegans* and mice to humans. Accumulation of Parkin in mitochondria, increased LC3II levels, and autophagic vesicles containing altered mitochondrial structures had also been found in the hippocampus of AD patients [30, 84] and in some cellular models [31], thereby confirming the AD relevance of our findings in PS1 M146L NSCs.

Mitochondrial dynamics can act as a functional regulatory point in coordinating a cellular redox state–attributed nuclear developmental program in NSCs [21]. It is known that a

deregulation of mitochondrial dynamics and its imbalance toward a chronically fragmented state, such as in AD [85], impairs the self-renewal capacity of stem cells and leads to a depletion of the stem cell pool. In the present work, we describe an impaired balance of mitochondrial fission and fusion proteins and mitochondrial morphology in PS1 M146L NSCs (Fig. 6) as it was previously described in AD patients [64]. Reduction in mitochondrial length is consistent with unopposed fission suggesting an altered mitochondrial dynamics in AD neurons [65, 86]. We should also note that in experiments with primary hippocampal neurons treated with Aβ-derived diffusible ligands (ADDLs), it was found that mitochondria in neurons are shortened and exhibit altered levels of fission and fusion proteins [64]. Similarly, mitochondria in pyramidal neurons of AD patients were abnormally redistributed away from axons [64]. We observed that PS1 M146L NSCs exhibited an abnormal mitochondrial morphology resulting in an increased mitochondrial fragmentation, with a prominent shift toward mitochondrial fission as a characteristic AD feature [85]. An increase in mitochondrial network fission may result in an increased abundance of dysfunctional mitochondria and increased ROS production [87]. It is also known that increased mitochondrial fragmentation alters the metabolic and respiratory profile of NSC due to its upstream regulation by mitochondrial dynamics [21].

Considering the above, we evaluated whether the treatment with bexarotene would be able to reverse the observed mitophagy and mitochondrial morphology abnormality in NSCs. Bexarotene is an FDA-approved retinoid X receptor (RXR) agonist for all stages of cutaneous T cell lymphoma [35]. Currently, it is in clinical trials in AD patients based on previous preclinical trial works in an AD mouse model [40, 88, 89]. These studies indicate the potential therapeutic efficacy of bexarotene stemming from increased Aβ clearance by PPARγ activation [90], an improved neural network function, and a reversal of behavioral deficits in mice [44, 91, 92]. In this study, we have evaluated the effect of bexarotene on the recovery of the autophagy impairment in our model of PS1 M146L NSCs. Bexarotene improved autophagic induction consistent with the upregulation of the TFEB, master regulator of autophagy, and the increased LC3 synthesis and degradation (Fig. 5a–e). These data correlated with the reduction of p62 levels as a result of the enhanced autophagy flux (Fig. 5f–h). Previous findings demonstrated that bexarotene enhanced autophagy and protected against thromboembolic stroke in aged transgenic mice expressing the human P301L-Tau mutation [93]. Moreover, a recent study demonstrated that bexarotene promoted neuroprotection by the regulation of PPARδ restoring affected mitochondrial respiration and quality control homeostasis in a model of Huntington's disease [94]. It is shown that the activation of PPARδ is also neuroprotective in a mouse model of AD through inhibition of inflammation [95]. We observed that bexarotene improves mitophagy as reflected by the recruitment of Parkin to mitochondria and its activation, to restore mitophagy (Fig. 6b, c). This decreased the abnormal accumulation of mitochondria (TOM20) (Fig. 6d, e) under basal conditions and after CCCP treatment, by the increased of autophagy vesicle synthesis. We also observed that bexarotene restored the expression of some complex I subunit and its activity in PS1 M146L cells (Fig. 6f, g). Moreover, bexarotene treatment induced an upregulation of the proteins involved in mitochondrial dynamics, which correlated with mitochondrial network morphology rescue and distribution (Fig. 7). It has been postulated that bexarotene acts by stimulating both LXR:RXR and PPARγ:RXR transcriptional activities [96, 97]. However, further studies are needed to determine the molecular pathway involved in the upregulation of autophagy and energetic changes in AD models.

Conclusions

In summary, our findings indicate that iPSC-derived PS1 M146L NSCs harboring *PS1* M146L mutation demonstrate a marked mitophagy failure associated with an autophagy induction blockage. We describe a deregulation of the expression of proteins involved in mitochondrial dynamics as well as an aberrant mitochondrial network morphology, suggesting an impairment in mitochondrial distribution and degradation. We also show that bexarotene treatment restores autophagy and can compensate mitochondrial anomalies in PS1 M146L NSCs, by enhancing the clearance of mitochondria. Our data support the hypothesis that pharmacologically induced mitophagy enhancement is a relevant and novel therapeutic strategy for the treatment of AD.

Acknowledgments We would like to thank Marc Tessier-Lavigne for supporting the generation of cell lines, Matt Zimmer for performing FACS on GFP/RFP double-transfected cells to help generate PS1 M146L knockin iPSCs, Brian Campos for technical assistance in screening candidate clones, and Ana Sevilla for performing iPSC immunostaining characterization.

Authors' Contributions PMM designed, performed, analyzed, and interpreted data as well as wrote the manuscript; AS, HM, DP, MTL CLM, and SN generated hiPSC-derived NSCs harboring the FAD-associated mutation. MG performed OXPHOS studies. AS and AAS contributed to data interpretation and manuscript editing. All authors read and approved the final manuscript.

Funding This work was supported by the NIA Grant P01AG014930 (A.A.S. and S.N.).

Compliance with Ethical Standards

Ethics Approval and Consent to Participate Human subject research at the New York Stem Cell Foundation was performed in accordance with applicable federal and state regulations, as well as with guidelines

established by the National Institutes of Health (NIH), National Academy of Sciences (NAS), and International Society for Stem Cell Research (ISSCR). It was also fully compliant with standards outlined in the Health Insurance Portability and Accountability Act (HIPAA) and in the Office for Human Research Protections (OHRP) recommendations.

Consent for Publication All authors declare their consent for publication of this manuscript.

Competing Interests The authors declare that they have no competing interests.

Abbreviations (AD), Alzheimer's disease; (Aβ), amyloid beta; (APP), amyloid beta (A4) precursor protein; (AVs), autophagic vacuoles; (Baf A1), bafilomycin A1; (CCCP), carbonyl cyanide m-chlorophenylhydrazone; (DLP1), dynamin-like protein 1; (FAD), familial Alzheimer's disease; (GAPDH), glyceraldehyde-3-phosphate dehydrogenase; (iPSC), induced pluripotent stem cells; HAR, hexaammineruthenium (III); (LAMP1), lysosomal-associated membrane protein 1; (MAP1LC3/LC3), microtubule-associated protein 1 light chain 3; (mtDNA), mitochondrial DNA; (MFN1), mitofusin 1; (MFN2), mitofusin 2; (NPCs), neural progenitor cells; (OPA1), optic atrophy 1; (OPTN), optineurin; (OXPHOS), oxidative phosphorylation system; (PSEN), presenilin; (PINK1), PTEN-induced putative kinase 1; (ROS), reactive oxygen species; (RXR), retinoid X receptor; (TFEB), transcription factor EB; (TOMM20), translocase of outer mitochondrial membrane 20 homolog

References

1. Hardy J, Selkoe DJ (2002) The amyloid hypothesis of Alzheimer's disease: progress and problems on the road to therapeutics. Science 297(5580):353–356
2. Holtzman DM et al (2011) Mapping the road forward in Alzheimer's disease. Sci Transl Med 3(114):114ps48
3. Klionsky DJ et al (2016) Guidelines for the use and interpretation of assays for monitoring autophagy (3rd edition). Autophagy 12(1):1–222
4. Ryan NS, Rossor MN (2010) Correlating familial Alzheimer's disease gene mutations with clinical phenotype. Biomark Med 4(1):99–112
5. Borchelt DR, Thinakaran G, Eckman CB, Lee MK, Davenport F, Ratovitsky T, Prada CM, Kim G et al (1996) Familial Alzheimer's disease-linked presenilin 1 variants elevate Abeta1-42/1-40 ratio in vitro and in vivo. Neuron 17(5):1005–1013
6. Zhao C, Deng W, Gage FH (2008) Mechanisms and functional implications of adult neurogenesis. Cell 132(4):645–660
7. Mu Y, Gage FH (2011) Adult hippocampal neurogenesis and its role in Alzheimer's disease. Mol Neurodegener 6:85
8. Demars M et al (2010) Impaired neurogenesis is an early event in the etiology of familial Alzheimer's disease in transgenic mice. J Neurosci Res 88(10):2103–2117
9. Li B et al (2008) Failure of neuronal maturation in Alzheimer disease dentate gyrus. J Neuropathol Exp Neurol 67(1):78–84
10. Wong PC, Zheng H, Chen H, Becher MW, Sirinathsinghji DJ, Trumbauer ME, Chen HY, Price DL et al (1997) Presenilin 1 is required for Notch1 and DII1 expression in the paraxial mesoderm. Nature 387(6630):288–292
11. Shen J, Bronson RT, Chen DF, Xia W, Selkoe DJ, Tonegawa S (1997) Skeletal and CNS defects in Presenilin-1-deficient mice. Cell 89(4):629–639
12. Chen Q, Nakajima A, Choi SH, Xiong X, Sisodia SS, Tang YP (2008) Adult neurogenesis is functionally associated with AD-like neurodegeneration. Neurobiol Dis 29(2):316–326
13. Haughey NJ et al (2002) Disruption of neurogenesis by amyloid beta-peptide, and perturbed neural progenitor cell homeostasis, in models of Alzheimer's disease. J Neurochem 83(6):1509–1524
14. Zhang C et al (2007) Long-lasting impairment in hippocampal neurogenesis associated with amyloid deposition in a knock-in mouse model of familial Alzheimer's disease. Exp Neurol 204(1):77–87
15. Lazarov O, Marr RA (2010) Neurogenesis and Alzheimer's disease: at the crossroads. Exp Neurol 223(2):267–281
16. Papa S et al (2004) Respiratory complex I in brain development and genetic disease. Neurochem Res 29(3):547–560
17. Calingasan NY et al (2008) Influence of mitochondrial enzyme deficiency on adult neurogenesis in mouse models of neurodegenerative diseases. Neuroscience 153(4):986–996
18. Kathleen Baxter K et al (2009) The neurogenic basic helix-loop-helix transcription factor NeuroD6 concomitantly increases mitochondrial mass and regulates cytoskeletal organization in the early stages of neuronal differentiation. ASN Neuro 1(4):195–211
19. Kirby DM, Rennie KJ, Smulders-Srinivasan TK, Acin-Perez R, Whittington M, Enriquez JA, Trevelyan AJ, Turnbull DM et al (2009) Transmitochondrial embryonic stem cells containing pathogenic mtDNA mutations are compromised in neuronal differentiation. Cell Prolif 42(4):413–424
20. Voloboueva LA, Giffard RG (2011) Inflammation, mitochondria, and the inhibition of adult neurogenesis. J Neurosci Res 89(12):1989–1996
21. Khacho M et al (2016) Mitochondrial dynamics impacts stem cell identity and fate decisions by regulating a nuclear transcriptional program. Cell Stem Cell 19(2):232–247
22. Bonda DJ, Wang X, Perry G, Nunomura A, Tabaton M, Zhu X, Smith MA (2010) Oxidative stress in Alzheimer disease: a possibility for prevention. Neuropharmacology 59(4–5):290–294
23. Lemasters JJ (2005) Selective mitochondrial autophagy, or mitophagy, as a targeted defense against oxidative stress, mitochondrial dysfunction, and aging. Rejuvenation Res 8(1):3–5
24. Youle RJ, Narendra DP (2011) Mechanisms of mitophagy. Nat Rev Mol Cell Biol 12(1):9–14
25. Narendra DP et al (2010) PINK1 is selectively stabilized on impaired mitochondria to activate Parkin. PLoS Biol 8(1):e1000298
26. Vives-Bauza C, Zhou C, Huang Y, Cui M, de Vries RLA, Kim J, May J, Tocilescu MA et al (2010) PINK1-dependent recruitment of Parkin to mitochondria in mitophagy. Proc Natl Acad Sci U S A 107(1):378–383
27. Geisler S et al (2010) PINK1/Parkin-mediated mitophagy is dependent on VDAC1 and p62/SQSTM1. Nat Cell Biol 12(2):119–131
28. Gegg ME, Cooper JM, Chau KY, Rojo M, Schapira AHV, Taanman JW (2010) Mitofusin 1 and mitofusin 2 are ubiquitinated in a PINK1/parkin-dependent manner upon induction of mitophagy. Hum Mol Genet 19(24):4861–4870
29. Bjorkoy G et al (2005) p62/SQSTM1 forms protein aggregates degraded by autophagy and has a protective effect on huntingtin-induced cell death. J Cell Biol 171(4):603–614
30. Martin-Maestro P et al (2016) PARK2 enhancement is able to compensate mitophagy alterations found in sporadic Alzheimer's disease. Hum Mol Genet 25(4):792–806
31. Martin-Maestro P et al (2017) Mitophagy failure in fibroblasts and iPSC-derived neurons of Alzheimer's disease-associated presenilin 1 mutation. Front Mol Neurosci 10:291
32. Moreira PI, Siedlak SL, Wang X, Santos MS, Oliveira CR, Tabaton M, Nunomura A, Szweda LI et al (2007) Increased autophagic degradation of mitochondria in Alzheimer disease. Autophagy 3(6):614–615

33. Moreira PI et al (2007) Autophagocytosis of mitochondria is prominent in Alzheimer disease. J Neuropathol Exp Neurol 66(6):525–532
34. Sodhi RK, Singh N (2014) Retinoids as potential targets for Alzheimer's disease. Pharmacol Biochem Behav 120:117–123
35. Henney JE (2000) From the Food and Drug Administration. JAMA 283(9):1131
36. Abba MC, Hu Y, Levy CC, Gaddis S, Kittrell FS, Zhang Y, Hill J, Bissonnette RP et al (2008) Transcriptomic signature of bexarotene (rexinoid LGD1069) on mammary gland from three transgenic mouse mammary cancer models. BMC Med Genet 1:40
37. McFarland K, Spalding TA, Hubbard D, Ma JN, Olsson R, Burstein ES (2013) Low dose bexarotene treatment rescues dopamine neurons and restores behavioral function in models of Parkinson's disease. ACS Chem Neurosci 4(11):1430–1438
38. Riancho J et al (2015) Neuroprotective effect of bexarotene in the SOD1(G93A) mouse model of amyotrophic lateral sclerosis. Front Cell Neurosci 9:250
39. Bomben V et al (2014) Bexarotene reduces network excitability in models of Alzheimer's disease and epilepsy. Neurobiol Aging 35(9):2091–2095
40. Cramer PE et al (2012) ApoE-directed therapeutics rapidly clear beta-amyloid and reverse deficits in AD mouse models. Science 335(6075):1503–1506
41. Moutinho M, Landreth GE (2017) Therapeutic potential of nuclear receptor agonists in Alzheimer's disease. J Lipid Res 58(10):1937–1949
42. Cummings JL et al (2016) Double-blind, placebo-controlled, proof-of-concept trial of bexarotene Xin moderate Alzheimer's disease. Alzheimers Res Ther 8:4
43. Pierrot N, Lhommel R, Quenon L, Hanseeuw B, Dricot L, Sindic C, Maloteaux JM, Octavea JN et al (2016) Targretin improves cognitive and biological markers in a patient with Alzheimer's disease. J Alzheimers Dis 49(2):271–276
44. Boehm-Cagan A, Michaelson DM (2014) Reversal of apoE4-driven brain pathology and behavioral deficits by bexarotene. J Neurosci 34(21):7293–7301
45. Sproul AA et al (2014) Characterization and molecular profiling of PSEN1 familial Alzheimer's disease iPSC-derived neural progenitors. PLoS One 9(1):e84547
46. Paquet D et al (2016) Efficient introduction of specific homozygous and heterozygous mutations using CRISPR/Cas9. Nature 533(7601):125–129
47. Rubinsztein DC, Cuervo AM, Ravikumar B, Sarkar S, Korolchuk VI, Kaushik S, Klionsky DJ (2009) In search of an "autophagomometer". Autophagy 5(5):585–589
48. Malik AN et al (2011) Mitochondrial DNA as a non-invasive biomarker: accurate quantification using real time quantitative PCR without co-amplification of pseudogenes and dilution bias. Biochem Biophys Res Commun 412(1):1–7
49. Sled VD, Vinogradov AD (1993) Kinetics of the mitochondrial NADH-ubiquinone oxidoreductase interaction with hexammineruthenium(III). Biochim Biophys Acta 1141(2–3):262–268
50. Chiang MC, Nicol CJ, Cheng YC, Lin KH, Yen CH, Lin CH (2016) Rosiglitazone activation of PPARgamma-dependent pathways is neuroprotective in human neural stem cells against amyloid-beta-induced mitochondrial dysfunction and oxidative stress. Neurobiol Aging 40:181–190
51. Manczak M, Park BS, Jung Y, Reddy PH (2004) Differential expression of oxidative phosphorylation genes in patients with Alzheimer's disease: implications for early mitochondrial dysfunction and oxidative damage. NeuroMolecular Med 5(2):147–162
52. Rhein V, Song X, Wiesner A, Ittner LM, Baysang G, Meier F, Ozmen L, Bluethmann H et al (2009) Amyloid-beta and tau synergistically impair the oxidative phosphorylation system in triple transgenic Alzheimer's disease mice. Proc Natl Acad Sci U S A 106(47):20057–20062
53. Stepanova A, Kahl A, Konrad C, ten V, Starkov AS, Galkin A (2017) Reverse electron transfer results in a loss of flavin from mitochondrial complex I: potential mechanism for brain ischemia reperfusion injury. J Cereb Blood Flow Metab 37(12):3649–3658
54. Kahl A, Stepanova A, Konrad C, Anderson C, Manfredi G, Zhou P, Iadecola C, Galkin A (2018) Critical role of flavin and glutathione in complex I-mediated bioenergetic failure in brain ischemia/reperfusion injury. Stroke 49(5):1223–1231
55. Napolitano G, Ballabio A (2016) TFEB at a glance. J Cell Sci 129(13):2475–2481
56. Puertollano R, Ferguson SM, Brugarolas J, Ballabio A (2018) The complex relationship between TFEB transcription factor phosphorylation and subcellular localization. EMBO J 37(11):e98804
57. Kim J et al (2011) AMPK and mTOR regulate autophagy through direct phosphorylation of Ulk1. Nat Cell Biol 13(2):132–141
58. Lee JH et al (2010) Lysosomal proteolysis and autophagy require presenilin 1 and are disrupted by Alzheimer-related PS1 mutations. Cell 141(7):1146–1158
59. Ryan TA, Tumbarello DA (2018) Optineurin: a coordinator of membrane-associated cargo trafficking and autophagy. Front Immunol 9:1024
60. Narendra DP, Youle RJ (2011) Targeting mitochondrial dysfunction: role for PINK1 and Parkin in mitochondrial quality control. Antioxid Redox Signal 14(10):1929–1938
61. Ni HM, Williams JA, Ding WX (2015) Mitochondrial dynamics and mitochondrial quality control. Redox Biol 4:6–13
62. Loson OC et al (2013) Fis1, Mff, MiD49, and MiD51 mediate Drp1 recruitment in mitochondrial fission. Mol Biol Cell 24(5):659–667
63. Palmer CS et al (2011) MiD49 and MiD51, new components of the mitochondrial fission machinery. EMBO Rep 12(6):565–573
64. Wang X, Su B, Lee HG, Li X, Perry G, Smith MA, Zhu X (2009) Impaired balance of mitochondrial fission and fusion in Alzheimer's disease. J Neurosci 29(28):9090–9103
65. Wang X, Su B, Fujioka H, Zhu X (2008) Dynamin-like protein 1 reduction underlies mitochondrial morphology and distribution abnormalities in fibroblasts from sporadic Alzheimer's disease patients. Am J Pathol 173(2):470–482
66. Martin-Maestro P et al (2017) Slower dynamics and aged mitochondria in sporadic Alzheimer's disease. Oxidative Med Cell Longev 2017:9302761
67. Smirnova E, Griparic L, Shurland DL, van der Bliek A (2001) Dynamin-related protein Drp1 is required for mitochondrial division in mammalian cells. Mol Biol Cell 12(8):2245–2256
68. Valente AJ, Maddalena LA, Robb EL, Moradi F, Stuart JA (2017) A simple ImageJ macro tool for analyzing mitochondrial network morphology in mammalian cell culture. Acta Histochem 119(3):315–326
69. Xia D, Watanabe H, Wu B, Lee SH, Li Y, Tsvetkov E, Bolshakov VY, Shen J et al (2015) Presenilin-1 knockin mice reveal loss-of-function mechanism for familial Alzheimer's disease. Neuron 85(5):967–981
70. Saura CA, Choi SY, Beglopoulos V, Malkani S, Zhang D, Rao BSS, Chattarji S, Kelleher RJ III et al (2004) Loss of presenilin function causes impairments of memory and synaptic plasticity followed by age-dependent neurodegeneration. Neuron 42(1):23–36
71. Wines-Samuelson M, Schulte EC, Smith MJ, Aoki C, Liu X, Kelleher RJ, Shen J (2010) Characterization of age-dependent and progressive cortical neuronal degeneration in presenilin conditional mutant mice. PLoS One 5(4):e10195
72. Veeraraghavalu K, Choi S, Zhang X, Sisodia SS (2013) Endogenous expression of FAD-linked PS1 impairs proliferation, neuronal differentiation and survival of adult hippocampal progenitors. Mol Neurodegener 8:41

73. Sherrington R et al (1995) Cloning of a gene bearing missense mutations in early-onset familial Alzheimer's disease. Nature 375(6534):754–760
74. Bruni AC et al (2010) Worldwide distribution of PSEN1 Met146Leu mutation: a large variability for a founder mutation. Neurology 74(10):798–806
75. Page RM, Baumann K, Tomioka M, Pérez-Revuelta BI, Fukumori A, Jacobsen H, Flohr A, Luebbers T et al (2008) Generation of Abeta38 and Abeta42 is independently and differentially affected by familial Alzheimer disease-associated presenilin mutations and gamma-secretase modulation. J Biol Chem 283(2):677–683
76. Kuusisto E, Suuronen T, Salminen A (2001) Ubiquitin-binding protein p62 expression is induced during apoptosis and proteasomal inhibition in neuronal cells. Biochem Biophys Res Commun 280(1):223–228
77. Kuusisto E, Salminen A, Alafuzoff I (2002) Early accumulation of p62 in neurofibrillary tangles in Alzheimer's disease: possible role in tangle formation. Neuropathol Appl Neurobiol 28(3):228–237
78. Fernandez-Mosquera L et al (2017) Acute and chronic mitochondrial respiratory chain deficiency differentially regulate lysosomal biogenesis. Sci Rep 7:45076
79. Tanaka A (2010) Parkin-mediated selective mitochondrial autophagy, mitophagy: Parkin purges damaged organelles from the vital mitochondrial network. FEBS Lett 584(7):1386–1392
80. Lonskaya I, Shekoyan AR, Hebron ML, Desforges N, Algarzae NK, Moussa CE (2013) Diminished parkin solubility and co-localization with intraneuronal amyloid-beta are associated with autophagic defects in Alzheimer's disease. J Alzheimers Dis 33(1):231–247
81. Witte ME, Bol JGJM, Gerritsen WH, Valk P, Drukarch B, Horssen J, Wilhelmus MMM (2009) Parkinson's disease-associated parkin colocalizes with Alzheimer's disease and multiple sclerosis brain lesions. Neurobiol Dis 36(3):445–452
82. Wang L et al (2016) Synaptosomal mitochondrial dysfunction in 5xFAD mouse model of Alzheimer's disease. PLoS One 11(3): e0150441
83. Fang EF et al (2019) Mitophagy inhibits amyloid-beta and tau pathology and reverses cognitive deficits in models of Alzheimer's disease. Nat Neurosci 22(3):401–412
84. Ye X et al (2015) Parkin-mediated mitophagy in mutant hAPP neurons and Alzheimer's disease patient brains. Hum Mol Genet 24(10):2938–2951
85. Garcia-Escudero V et al (2013) Deconstructing mitochondrial dysfunction in Alzheimer disease. Oxidative Med Cell Longev 2013: 162152
86. Wang X, Su B, Siedlak SL, Moreira PI, Fujioka H, Wang Y, Casadesus G, Zhu X (2008) Amyloid-beta overproduction causes abnormal mitochondrial dynamics via differential modulation of mitochondrial fission/fusion proteins. Proc Natl Acad Sci U S A 105(49):19318–19323
87. Knott AB, Perkins G, Schwarzenbacher R, Bossy-Wetzel E (2008) Mitochondrial fragmentation in neurodegeneration. Nat Rev Neurosci 9(7):505–518
88. Veeraraghavalu K, Zhang C, Miller S, Hefendehl JK, Rajapaksha TW, Ulrich J, Jucker M, Holtzman DM et al (2013) Comment on "ApoE-directed therapeutics rapidly clear beta-amyloid and reverse deficits in AD mouse models". Science 340(6135):924–92f
89. Ulrich JD, Burchett JM, Restivo JL, Schuler DR, Verghese PB, Mahan TE, Landreth GE, Castellano JM et al (2013) In vivo measurement of apolipoprotein E from the brain interstitial fluid using microdialysis. Mol Neurodegener 8(8):13
90. Mandrekar-Colucci S, Landreth GE (2011) Nuclear receptors as therapeutic targets for Alzheimer's disease. Expert Opin Ther Targets 15(9):1085–1097
91. Tesseur I et al (2013) Comment on "ApoE-directed therapeutics rapidly clear beta-amyloid and reverse deficits in AD mouse models". Science 340(6135):924-e
92. Fitz NF, Cronican AA, Lefterov I, Koldamova R (2013) Comment on "ApoE-directed therapeutics rapidly clear beta-amyloid and reverse deficits in AD mouse models". Science 340(6135):924–92c
93. Huuskonen MT et al (2016) Bexarotene targets autophagy and is protective against thromboembolic stroke in aged mice with tauopathy. Sci Rep 6:33176
94. Dickey AS, Sanchez DN, Arreola M, Sampat KR, Fan W, Arbez N, Akimov S, van Kanegan MJ et al (2017) PPARdelta activation by bexarotene promotes neuroprotection by restoring bioenergetic and quality control homeostasis. Sci Transl Med 9(419):eaal2332
95. Malm T, Mariani M, Donovan LJ, Neilson L, Landreth GE (2015) Activation of the nuclear receptor PPARdelta is neuroprotective in a transgenic mouse model of Alzheimer's disease through inhibition of inflammation. J Neuroinflammation 12:7
96. Yamanaka M, Ishikawa T, Griep A, Axt D, Kummer MP, Heneka MT (2012) PPARgamma/RXRalpha-induced and CD36-mediated microglial amyloid-beta phagocytosis results in cognitive improvement in amyloid precursor protein/presenilin 1 mice. J Neurosci 32(48):17321–17331
97. Mandrekar-Colucci S, Karlo JC, Landreth GE (2012) Mechanisms underlying the rapid peroxisome proliferator-activated receptor-gamma-mediated amyloid clearance and reversal of cognitive deficits in a murine model of Alzheimer's disease. J Neurosci 32(30): 10117–10128